JGR Oceans

RESEARCH ARTICLE
10.1029/2020JC016610

Particulate Scattering and Backscattering in Relation to the Nature of Particles in the Red Sea

Malika Kheireddine[1], **R. J. W. Brewin**[2], **M. Ouhssain**[1], **and B. H. Jones**[1]

[1]Red Sea Research Center (RSRC), King Abdullah University of Science and Technology (KAUST), Biological and Environmental Sciences and Engineering Division (BESE), Thuwal, Saudi Arabia, [2]College of Life and Environmental Sciences, University of Exeter, Penryn Campus Cornwall, UK

Key Points:

- The first measurements of particulate backscattering and scattering coefficients were collected over wide spatial scales in the Red Sea
- We fit conceptual models to relate particulate backscattering and scattering to chlorophyll-a assuming three different populations of particles
- The backscattering ratio of the background component is high and dominated by non-algal particles

Correspondence to:
M. Kheireddine,
malika.kheireddine@kaust.edu.sa

Citation:
Kheireddine, M., Brewin, R. J. W., Ouhssain, M., & Jones, B. H. (2021). Particulate scattering and backscattering in relation to the nature of particles in the Red Sea. *Journal of Geophysical Research: Oceans*, *126*, e2020JC016610. https://doi.org/10.1029/2020JC016610

Received 17 JUL 2020
Accepted 6 FEB 2021

Abstract Measurements of light scattering can be used to quantify the concentration and composition of oceanic particles, and resolve biogeochemical processes spanning different time and space scales. In this paper, we analyze the first dataset, collected over wide spatial scales in the Red Sea, of particulate scattering ($b_p(\lambda)$), particulate backscattering ($b_{bp}(\lambda)$), particulate absorption and chlorophyll-a concentration [Chl_a]. We fit a three-component conceptual model relating $b_{bp}(\lambda)$ to [Chl_a], assuming a fixed background component ($b_{bp}^{k}(\lambda)$), and two additional components driven by small (<2 μm) and large phytoplankton (>2 μm) ($b_{bp,1}(\lambda)$ and $b_{bp,2}(\lambda)$, respectively). We extend the approach, for the first time, to the modeling of total particulate scattering ($b_p(\lambda)$), allowing us to retrieve the backscattering ratio for each component in the model. We observe a high backscattering ratio for the background component which, when analyzed alongside measurements of particulate absorption, suggests it is likely dominated by non-algal (rather than algal) particles. The high contribution of non-algal particles to $b_{bp}(\lambda)$ at low [Chl_a] may be related to the unique conditions in the Red Sea, or more broadly, characteristic of other oceanic conditions. The work illustrates how we can combine optical measurements with conceptual models, to understand better the composition of oceanic particles and ultimately, improve monitoring of marine biogeochemical processes. Our work will also be useful for developing regional ocean-color models for the Red Sea.

Plain Language Summary The ocean contains a large variety of suspended particles that cover a broad size range, from 0.1 nm to 1 mm, and vary in origin, shape and internal composition. The pool of suspended particles is often divided into non-algal particles and phytoplankton. Most particles play an important role in ocean processes like primary production that modulate the biological carbon pump in the ocean. Concentration and various type of marine particles can be estimated and studied from measurements of light scattering (i.e., particulate backscattering and scattering), and help study and understand biogeochemical processes in aquatic environments. However, separating the contribution from non-algal particles and phytoplankton to scattering properties is challenging given they often co-vary with phytoplankton biomass in open ocean waters. The particulate backscattering and scattering coefficients were fit to a chlorophyll-a dependent conceptual model that assumed three components: A background component, and small and large phytoplankton populations. We found that the background population is likely dominated by non-algal, rather than algal, particles, which has a major impact on backscattering in Red Sea waters. Our results will help interpret ocean-color remote sensing data to help study marine biogeochemical processes in the Red Sea.

1. Introduction

The ocean contains a large variety of suspended particles that cover a broad size range, from 0.1 nm to 1 mm, and vary in origin (i.e., biogenic or terrestrial), shape and internal composition (i.e., refractive index; Stramski et al., 2004). The pool of suspended particles is often divided into non-algal particles and phytoplankton. Non-algal particles include: (1) heterotrophs (i.e., bacteria, viruses and zooplankton), (2) non-living organic detritus produced by zoo- and phyto-plankton (i.e., fecal pellets, dead cells), and (3) mineral particles (e.g., silicate shells, dusts, clay, etc.). The phytoplankton pool is often divided according to cell size (Sieburth et al., 1978), into pico-phytoplankton (0.2–2 μm), nano-phytoplankton (2–20 μm) and micro-phytoplankton

(>20 μm), owing to the strong link between size and ecological function (Marañón, 2019). Most particles play an important role in ocean processes like primary production, export and recycling, that modulate the biological carbon pump (BCP, defined as the transfer of organic carbon from the surface ocean to the deep ocean). Several deep ocean ecosystems rely on the BCP as an energy source, like mesopelagic fish ecosystems upon which humans depend. The BCP is also a vital component of the ocean carbon cycle controlling the ocean's capacity to regulate the concentration of atmospheric CO_2 (Briggs et al., 2020; Kwon et al., 2009).

Measurements of light scattering by marine particles (i.e., particulate scattering ($b_p(\lambda)$) and particulate backscattering ($b_{bp}(\lambda)$) measurements) can be used to quantify the concentration of various types of particles, and help study and understand BCP processes (Bishop et al., 2002; Briggs et al., 2020, 2011; Dall'Olmo & Mork, 2014; Dall'Olmo et al., 2016; Estapa et al., 2019, 2017; Kheireddine & Antoine, 2014; Kheireddine et al., 2020). Thanks to advances in technology, scattering measurements can be acquired from autonomous underwater vehicles (i.e. gliders and profiling floats using scattering sensors), and inferred from satellite measurements of ocean color, though the use of bio-optical inversion algorithms. These tools are helping to understand the functioning of the ocean ecosystem over a span of time and space scales, ranging from diurnal to inter-annual, and in different areas of the global ocean.

To understand how scattering properties vary with phytoplankton concentration, studies have looked at the relationship between $b_p(\lambda)$ and $b_{bp}(\lambda)$ and the chlorophyll-a concentration ([Chl_a]), a proxy of phytoplankton abundance (Antoine et al., 2011; Bellacicco et al., 2019; Brewin et al., 2012; Dall'Olmo et al., 2012; Huot et al., 2008). Separating the contribution from non-algal particles and phytoplankton to scattering properties is challenging given they often co-vary with [Chl_a] in open ocean waters (Antoine et al., 2011; Huot et al., 2008; Loisel et al., 2007). The backscattering ratio (i.e., the ratio of scattering to backscattering, at a given wavelength $(\lambda)\frac{b_{bp}}{b_p}$) has been used to provide information on the particle's size and composition (Antoine et al., 2011; Loisel et al., 2007; Twardowski et al., 2001; Xi et al., 2015), and has the potential to help separate the contribution from non-algal particles and phytoplankton, given its sensitivity to the size and refractive index of particles, which can vary between algal and non-algal particles. It has been also used for radiative transfer simulations and the development of algorithms to retrieve biogeochemical quantities from ocean-color remote sensing (Morel & Maritorena, 2001).

Studies have explored the possibility of estimating the background contribution of non-algal particles to $b_{bp}(\lambda)$ by extracting the fraction that does not co-vary with [Chl_a] (Behrenfeld et al., 2005; Bellacicco et al., 2019; Brewin et al., 2012; Zhang et al., 2020). Of these approaches, Brewin et al. (2012) modeled the relationship between $b_{bp}(\lambda)$ and [Chl_a] assuming three component populations, a background component, where $b_{bp}(\lambda)$ does not co-vary with [Chl_a], particle populations dominated by small phytoplankton and their co-varying material, and particle populations dominated by large phytoplankton and their co-varying material. Bellacicco et al. (2019) applied this model to biogeochemical-Argo float data to investigate global variations in the background contribution of particles to $b_{bp}(\lambda)$, by making the assumption the background component of the Brewin et al. (2012) model ($b_{bp}^k(\lambda)$) is dominated by non-algal particles.

The Red Sea, the northernmost tropical sea of the global ocean, is among the most saline and warmest seas on the planet (Chaidez et al., 2017; Kheireddine et al., 2018), and is thought to be representative of conditions that may occur in wide areas of the global ocean in the future, in the context of climate change (Belkin, 2009; Breitburg et al., 2018). The Red Sea is also fringed by coral reefs and mangroves teeming with life, with large marine biodiversity and unique ecological niches (Baars et al., 1998). The phytoplankton, ubiquitous in the global ocean, play a key role in the Red Sea ecosystem's functioning. At the base of the marine food web, phytoplankton are an important source of energy for the ecosystem. They support a chain of biogeochemical processes, collectively named the biological carbon pump, which is a vital component of the carbon cycle controlling the concentration of atmospheric CO_2 and regulating the rate of climate change (Boyd et al., 2019). The region is arid and characterized by low precipitation, little riverine input and significant inputs from dust (Al-Taani et al., 2015; Ginoux et al., 2012; Prakash et al., 2015; Prospero et al., 2002). While variations in $b_p(\lambda)$ and $b_{bp}(\lambda)$ have been

studied extensively in some areas of the global ocean (Behrenfeld et al., 2005; Brewin et al., 2012; Dall'Olmo et al., 2012; Huot et al., 2008; Loisel et al., 2007), only a few measurements of $b_{bp}(\lambda)$ have been obtained at specific locations in the Red Sea (Organelli et al., 2017) during the last 3 decades. Until now, no datasets of $b_{bp}(\lambda)$ were available over wide spatial scales in the Red Sea.

Recently, Brewin et al. (2015) tuned the Brewin et al. (2012) model to Red Sea waters to estimate the contribution of the background component and the chlorophyll-specific backscattering coefficients of environments dominated by pico-phytoplankton (<2 μm) and nano-micro-phytoplankton (>2 μm). However, due to the scarcity of in situ measurements of $b_{bp}(\lambda)$ and [Chl_a] at that time, they inferred $b_{bp}(\lambda)$ from particulate attenuation and absorption measurements, making assumptions on the backscattering ratio (Twardowski et al., 2001), and using the absorption line-height methods to derive [Chl_a] (Werdell et al., 2013). Since that study, in situ measurements of [Chl_a] by HPLC (Kheireddine et al., 2017, 2018), and in situ $b_{bp}(\lambda)$ and $b_p(\lambda)$ measurements, have been collected in Red Sea waters, providing the feasibility to tune the Brewin et al. (2012, 2015) model to direct observations in the Red Sea, and extend the approach to the modeling of total scattering. By doing so, there is potential to use the backscattering ratio to infer information regarding particle composition and type, for the three populations.

In this study, we make use of the first (to our knowledge) in situ dataset of scattering and [Chl_a] measurements collected over extensive areas in the Red Sea, to test and evaluate the model of Brewin et al. (2012; 2015) and, for the first time, extend the approach to the modeling of total scattering. By doing this, our goal is to: 1) improve our understanding of the nature of the particles in the Red Sea; and 2) improve our understanding of relationships between particles and optics in the region, with a view toward advancing ocean-color models for the Red Sea.

2. Materials and Methods

2.1. Study Area and Sampling

Samples were collected during four research cruises across the Red Sea between October 2014 and April 2015 on board of the R/V Thuwal. Two cruises named as CRS-01 and CRS-02, took place in the central Red Sea (CRS) during fall and spring, specifically from 16–28 October 2014 and from 29 March- 03 April 2015, respectively. One cruise, Duba-01, was conducted in the northern Red Sea (NRS) in spring from of 17–28 April 2015. A cruise to Jazan took place in the southern Red Sea (SRS) in winter from 8–21 February 2015. A total of 40 stations were sampled from surface to 200 m depth along the basin (Figure 1, Table 1). Temperature and salinity profiles were obtained using a SBE 9 (Sea-Bird Electronics) Conductivity-Temperature-Depth (CTD) probe.

2.2. Discrete Seawater Samples

Phytoplankton pigment concentrations and particulate absorption spectra were collected for some of the stations (26 in total) using a rosette system equipped with 10 L Niskin bottles at typically 10–12 depths (5, 10, 20, 40, 50, 60, 70, 80, 120, 150, 180 and 200 m) within the upper 200 m of the water column (Table 1).

2.3. Chlorophyll-a

Seawater samples (with volume ranging from 2.3 to 2.8 L) were filtered through 25 mm diameter Whatman GF/F filters (0.7 μm porosity), stored in liquid nitrogen during the cruise and subsequently at −80 °C in the laboratory until analysis. A total of 25 pigments were quantified using a High Performance Liquid Chromatography (HPLC), using a 1260 Agilent Technologies system, according to the protocol described in Ras et al. (2008) and Kheireddine et al. (2018). The missing [Chl_a] measurements (remaining 14 stations) [Chl_a] were obtained from the chlorophyll fluorescence modified into equivalent chlorophyll concentrations based on the HPLC measurements, using a power function ($R^2 = 0.93$, and root mean square = 0.11 in $\log_{10}$ space).

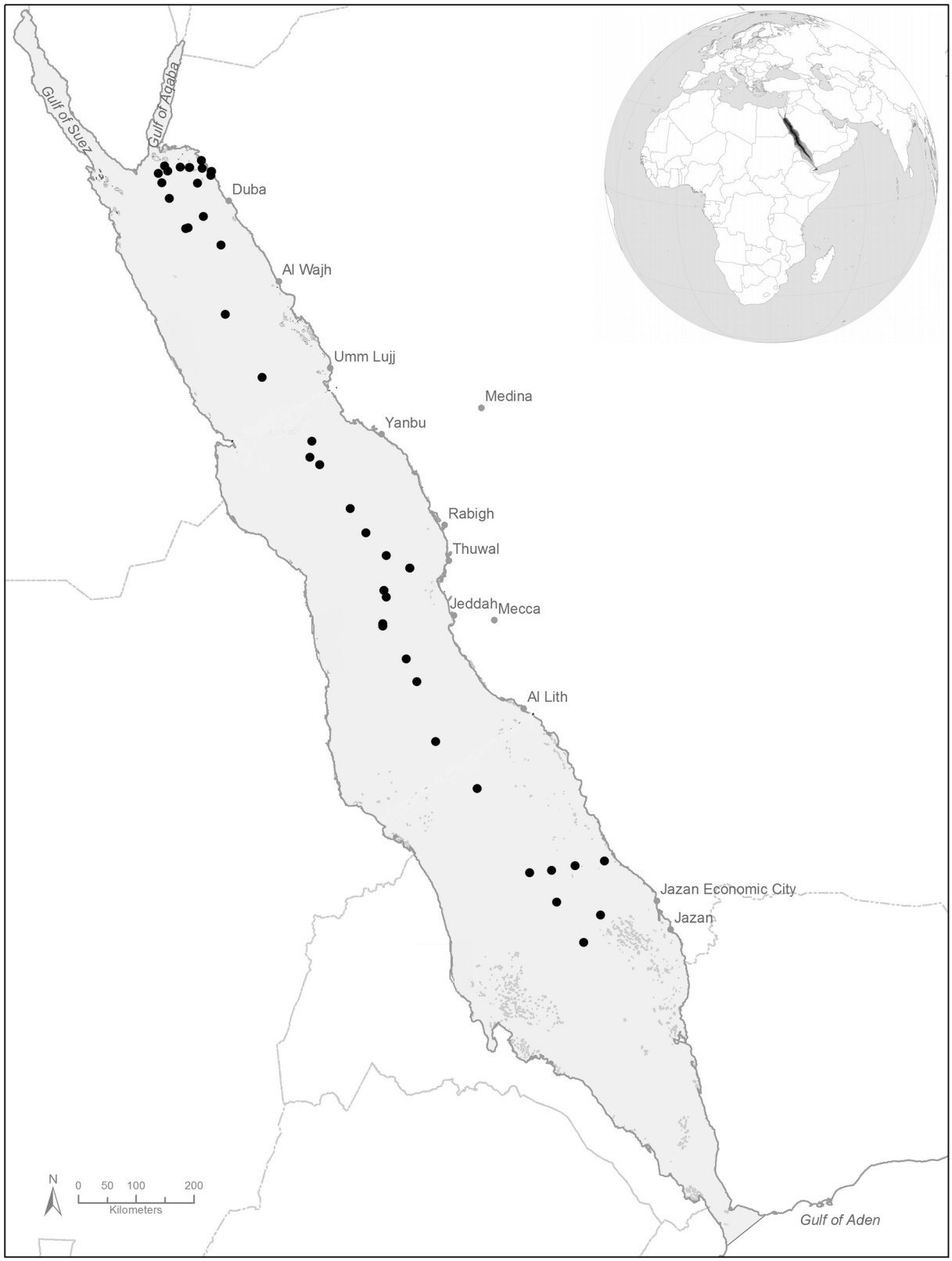

Figure 1. Location of stations sampled during the different cruises performed in the Red Sea between October 2014 and April 2015 (see Table 1). Map produced using ArcGIS.

Table 1
Number, Location and Area of the Stations Sampled During the Different Cruises and the Range in Measured Values of [Chl_a], $c_{p\,(650)}$, $b_{p\,(650)}$, $b_{bp\,(650)}$ and $\frac{a_{nap}(440)}{a_p(440)}$ Found in the Red Sea.

Campaign	Platform	Location	Abbreviation	Period	Number of stations	[Chl_a] ($mg.m^{-3}$)	$c_{p\,(650)}$ (m^{-1})	$b_{p\,(650)}$ (m^{-1})	$b_{bp\,(650)}$ (m^{-1})	$\frac{a_{nap}(440)}{a_p(440)}$
Nutrient cycle cruise 1	RV *Thuwal*	Central Red Sea	CRS-01	16–28 October 2014	8					
Jazan cruise	RV *Thuwal*	Southern Red Sea	Jazan	8–21 February 2015	8					
Nutrient cycle cruise 2	RV *Thuwal*	Central Red Sea	CRS-02	29 March–03 April 2015	6	0.04–0.75	0.03–0.25	0.03–0.22	0.0007–0.0027	0.04–0.80
Duba cruise	RV *Thuwal*	Northern Red Sea	Duba-01	17–28 April 2015	18					
Total					40					

2.4. a_{nap} and a_p Measurements

Particulate absorption spectra, $a_p(\lambda)$, were measured using a quantitative filter pad technique (Mitchell et al., 2003). Seawater samples (2.3 –2.8 L) were filtered on Whatman GF/F filters (0.7 μm porosity) and stored in liquid nitrogen during the cruise and subsequently at −80 °C in the laboratory until analysis (Organelli et al., 2013). The respective contributions of phytoplankton ($a_{ph}(\lambda)$) and non-algal particles ($a_{nap}(\lambda)$) to total particulate absorption were determined by numerical decomposition (Bricaud & Stramski, 1990) for most of the samples. A few samples have been analyzed using the method of Kishino et al. (1985), based on the pigment extraction in methanol and showed that absorption ratios derived from these $a_{ph}(\lambda)$ spectra were found to be very close to the standard ratios used in the numerical decomposition. Detailed information regarding the analyses of $a_p(\lambda)$, $a_{ph}(\lambda)$ and $a_{nap}(\lambda)$ can be found in Kheireddine et al. (2018).

2.5. b_{bp}, c_p and b_p Measurements

During each station, an instrument package with a set of sensors was deployed to obtain vertical profiles of optical measurements from surface to 200 m. The particle spectral backscattering measurements were determined with an ECO BB-9 backscattering sensor (Wet Labs, sampling rate 1 Hz) and; the particle spectral attenuation and scattering were determined with an ac-s hyper-spectral spectrophotometer (Wet Labs, sampling rate 4 Hz). Data from all instruments are merged and time-stamped using a WET Labs (Philomath, OR) DH-4 data handler with WET Labs Archive Protocol (WAP) software. All optical measurements from all sensors were median-binned into 1 meter intervals before further processing. Note that the sensors were calibrated on a regular basis before or after each cruise.

The ECO BB-9 backscattering sensor provides the volume scattering function at an angle of 124° ($\beta(124°,\lambda)$, where λ is the wavelength) and at wavelengths of 412, 440, 488, 510, 532, 595, 650, 676 and 715 nm. While the BB-9 instrument was calibrated by WET Labs on a yearly basis, dark counts determinations were performed prior and during the cruise every 2 to 3 stations by covering the detectors with black tape and submerging the instrument in water. In general, variations in the dark counts were small and close to those provided by the manufacturer. Scaling factors provided by Wet Labs and dark counts performed prior and during the cruise were then used to calculate $\beta(124°,\lambda)$, which represents the sum of the particle scattering plus the molecular scattering by the seawater for each wavelength. To obtain the volume scattering function of particles, $\beta_p(124°,\lambda)$, the volume scattering function of water $\beta_w(124°,\lambda)$ calculated using the temperature and salinity from the CTD measurements (obtained according to the relationship in Zhang et al. [2009]) is subtracted from $\beta(124°,\lambda)$. The particulate backscattering coefficient, $b_{bp}(\lambda)$ (m^{-1}), is then determined from $\beta_p(124°,\lambda)$ using a χ factor:

$$b_{bp}(\lambda) = 2\pi\chi\beta_p(124°,\lambda). \quad (1)$$

Based on Sullivan et al. (2013), the χ factor has been assumed to be 1.076 at all wavelengths.

Finally, vertical profile of b_{bp} were median-filtered to remove spikes (Briggs et al., 2011) and median-binned into 1 m depth for analysis and correlation with discrete water samples.

2.6. c_p and b_p Measurements

Hyperspectral total absorption and attenuation ($a(\lambda)$ and $c(\lambda)$) were measured on unfiltered bulk seawater using a WET Labs ac-s hyper-spectral spectrophotometer, and soluble absorption and attenuation were measured after filtration through a 0.2 μm filter (Whatman Polycap 75 TC) positioned at the intake of a second ac-s sensor, both linked to a SBE 49 FastCAT (Sea-Bird Electronics) CTD probe. The 0.2 μm filter was changed every 3 to 4 profiles within each cruise. The ac-s instruments provided spectral $a(\lambda)$ and $c(\lambda)$ at 81 wavelengths from 400 to 740 nm. A milli-Q water calibration was carried out prior to and after each cruise for each sensor, to facilitate cross-calibrations.

Particulate absorption and attenuation coefficient were calculated as follows:

$$a_p(\lambda) = a(\lambda) - a_{0.2\,\mu m}(\lambda), \quad (2)$$

$$c_p(\lambda) = c(\lambda) - c_{0.2\,\mu m}(\lambda), \quad (3)$$

where $a_p(\lambda)$ and $c_p(\lambda)$ are particulate absorption and attenuation, $a(\lambda)$ and $c(\lambda)$ are total absorption and attenuation and, $a_{0.2\,\mu m}(\lambda)$ and $c_{0.2\,\mu m}(\lambda)$ are the filtered portion, respectively. A scattering and residual temperature correction, using the temperature correction tables of Sullivan et al. (2006), were performed to consider for eventual dissimilarities in temperature and scattering between the filtered measurements and total measurements (Slade et al., 2010). To do so, we used the near-infrared region to correct absorption spectra for the effects of temperature and particle scattering, which lead to a correction of $0.007 \pm 0.003\ m^{-1}$. Any spectra that were either too noisy or characterized with obvious spectral artifacts were discarded. To match up with the ECO-BB9 wavelengths, $a_p(\lambda)$ and $c_p(\lambda)$ were linearly interpolated into 1 nm interval.

The particulate scattering was then estimated as follows:

$$b_p(\lambda) = c_p(\lambda) - a_p(\lambda). \quad (4)$$

Knowing the limitations of using ac-s measurements to infer $b_p(\lambda)$ measurements, we applied several scattering corrections for $a_p(\lambda)$ measurements and found that they had little impact on $b_p(\lambda)$ given that $c_p(\lambda)$ is dominated by $b_p(\lambda)$. This resulted in $b_p(\lambda)$ measurements with an uncertainty less than 5 %.

After correction and calculation, all absorption, attenuation, scattering measurements data for each vertical profile were median-binned to 1 meter interval to remove spikes for analysis and correlation with discrete water samples. Finally, the particle size distribution slope (PSD slope) was estimated from the spectral dependency of c_p using the approach of Boss et al. (2001).

2.7. Particulate Backscattering Ratio

The particulate backscattering ratio, was computed as follows:

$$\tilde{b}_{bp}(\lambda) = \frac{b_{bp}(\lambda)}{b_p(\lambda)}, \quad (5)$$

Table 2
Parameters Used for the Red Sea Models ($b_{bp}(\lambda)$ and $b_p(\lambda)$)

Parameters	Values
Parameters from Gittings et al. (2019) (Table 2)	
$[Chl\_a]$ (mg m^{-3})	0.19 (0.16 to 0.23)
S_1 (Dimensionless)	4.84 (4.35 to 5.31)
$b_{bp}(\lambda)$	
Parameters derived from Equations 11 and 12 in this study	
$b^*_{bp,1}(\lambda_0)$ (m^2 mg^{-1})	0.00274 (0.00235 to 0.00314)
$b^*_{bp,2}(\lambda_0)$ (m^2 mg^{-1})	0.002618 (0.00246 to 0.00304)
$b^k_{bp}(\lambda_0)$ (m^{-1})	0.001089 (0.001001 to 0.00112)
γ^1 (Dimensionless)	1.919 (0.834 to 2.943)
γ^2 (Dimensionless)	−0.106 (−0.098 to −0.115)
γ^k (Dimensionless)	0.786 (0.638 to 1.048)
$b_p(\lambda)$	
Parameters derived from Equations 13 and 14 in this study	
$b^*_{p,1}(\lambda_0)$ (m^2 mg^{-1})	0.542 (0.497 to 0.589)
$b^*_{p,2}(\lambda_0)$ (m^2 mg^{-1})	0.207 (0.186 to 0.225)
$b^k_{bp}(\lambda_0)$ (m^{-1})	0.055 (0.050 to 0.060)
η^1 (Dimensionless)	0.77 (0.69 to 0.86)
η^2 (Dimensionless)	0.18 (0.14 to 0.22)
η^k (Dimensionless)	1.67 (1.52 to 1.83)

Note. Values between brackets represent 95% confidence intervals and $\lambda 0 = 440$ nm.

and is a useful parameter providing information about the particulate composition (i.e., dominance of organic or inorganic particles in seawater) (Boss et al., 2004; Koestner et al., 2018; Twardowski et al., 2001)), acknowledging that these optical properties can be sensitive to different size ranges, according to some theoretical models (Morel & Ahn, 1991; Stramski & Kieffer, 1991).

2.8. Model

To interpret variations in $b_{bp}(\lambda)$ in relation to [Chl_a], we first partitioned [Chl_a] into two different size classes of phytoplankton (i.e., small and large) following a two-component model for determining the concentrations of large phytoplankton cells ($[\mathrm{Chl\_a}]_2$) and small phytoplankton cells ($[\mathrm{Chl\_a}]_1$) as follows:

$$[Chl\_a] = [Chl\_a]_1 + [Chl\_a]_2, \tag{6}$$

$$[Chl\_a]_1 = [Chl\_a]_1^m \,[1 - \exp(-S_1[Chl\_a])], \tag{7}$$

$$[Chl\_a]_2 = [Chl\_a] - [Chl\_a]_1. \tag{8}$$

Where subscript 1 refers to pico-phytoplankton size and subscript 2 refers to combined nano-micro-phytoplankton, $[\mathrm{Chl\_a}]_1^m$ represents the asymptotic maximum chlorophyll concentration for the pico-phytoplankton, and S_1 determines the initial increase in the chlorophyll concentration of pico-phytoplankton with [Chl_a]. These two parameters have been computed from the HPLC measurements collected in the Red Sea (Kheireddine et al., 2017, 2018) and are provided in Gittings et al. (2019, Table 2).

Then, we expressed $b_{bp}(\lambda)$ as follows:

$$b_{bp}(\lambda) = b_{bp,1}(\lambda) + b_{bp,2}(\lambda) + b^k_{bp}(\lambda). \tag{9}$$

Where $b_{bp,1}(\lambda)$ represents the contribution to particle backscattering by pico-phytoplankton and their co-varying constituents; $b_{bp,2}(\lambda)$, the contribution to particle backscattering by large phytoplankton (nano- and micro-phytoplankton) and their co-varying constituents; and $b^k_{bp}(\lambda)$, the contribution to particle backscattering by a constant background population of non-algal particles and potentially very small phytoplankton (e.g., *Prochlorococcus*). $b_{bp}(\lambda)$ can then be partitioned following Brewin et al. (2015):

$$b_{bp}(\lambda) = b^*_{bp,1}(\lambda)[Chl\_a]_1 + b^*_{bp,2}(\lambda)[Chl\_a]_2 + b^k_{bp}(\lambda). \tag{10}$$

Where $b^*_{bp,1}(\lambda)$ and $b^*_{bp,2}(\lambda)$ are the chlorophyll-specific particle backscattering coefficient of small (i.e., pico-) and large (i.e., nano-micro-) phytoplankton dominated waters, respectively.

By embedding the two-component model (Equations 6–8) into Equation 10, we obtain:

$$b_{bp}(\lambda) = [Chl\_a]_1^m \left[b^*_{bp,1}(\lambda) - b^*_{bp,2}(\lambda)\right]\left[1 - \exp\left(-S_1[Chl\_a]\right)\right] + b^*_{bp,2}(\lambda)[Chl\_a] + b^k_{bp}(\lambda). \tag{11}$$

Table 3
Range in $b_{bp}(\lambda)$ at Low [Chl_a] Concentrations (0.03–0.09 mg m^{-3}) Presented in Figure 2

λ (nm)	b_{bp} range (m^{-1})
440	0.0010 to 0.0015
532	0.0009 to 0.0013
650	0.0007 to 0.0011
715	0.0006 to 0.0010

Following Brewin et al. (2012, 2015), $b^*_{bp,1}(\lambda)$, $b^*_{bp,2}(\lambda)$ and $b^k_{bp}(\lambda)$ were estimated by fitting the above equation to our measurements of $b_{bp}(\lambda)$ and [Chl_a] using a non-linear least squares method (R, package "mosaic", function "fitModel") in conjunction with bootstrapping to estimate the parameters and their associated uncertainties. Bootstrapping was implemented by randomly re-sampling the dataset to create 5000 new dataset of the same size as the original and re-fitting the data for each to obtain a distribution of $b^*_{bp,1}(\lambda)$, $b^*_{bp,2}(\lambda)$ and $b^k_{bp}(\lambda)$. The median and the 95% confidence intervals were then computed from each of the resulting parameter distribution and are provided in Table 2.

As described in Brewin et al. (2012, 2015), the spectral dependency of $b^*_{bp,1}(\lambda)$, $b^*_{bp,2}(\lambda)$ and $b^k_{bp}(\lambda)$ was assumed to follow a power function, and thus Equation 11 can be expanded to the following expression:

$$b_{bp}(\lambda) = b^*_{bp,1}(\lambda_0)(\lambda / \lambda_0)^{-\gamma_1}\left\{\left[Chl\_a\right]_1^m\left[1-\exp\left(-S_1\left[Chl\_a\right]\right)\right]\right\} + b^*_{bp,2}(\lambda_0)(\lambda / \lambda_0)^{-\gamma_2}\left\{\left[Chl\_a\right]-\left[Chl\_a\right]_1^m\left[1-\exp\left(-S_1\left[Chl\_a\right]\right)\right]\right\} + b^k_{bp}(\lambda_0)(\lambda / \lambda_0)^{-\gamma_k}, \quad (12)$$

where γ_1, γ_2 and γ_k are the spectral dependency of $b^*_{bp,1}(\lambda)$, $b^*_{bp,2}(\lambda)$ and $b^k_{bp}(\lambda)$, respectively, and $\lambda_0 = 440$ nm. Knowing the distribution of $b^*_{bp,1}(\lambda)$, $b^*_{bp,2}(\lambda)$ and $b^k_{bp}(\lambda)$ and [Chl_a], the parameters γ_1, γ_2 and γ_k were simply estimated by fitting a wavelength-dependent power function in association with the bootstrapped $b^*_{bp,1}(\lambda)$, $b^*_{bp,2}(\lambda)$, and $b^k_{bp}(\lambda)$ values. The parameters and their uncertainties are provided in Table 2. Next, we extended the model of Brewin et al. (2015) to consider total scattering, and retrieve, for the first time, the contributions of the background population to total scattering, $b^k_p(\lambda)$, and the chlorophyll-specific scattering coefficients associated with environments dominated by pico-phytoplankton (<2 μm) and nano-micro-phytoplankton (>2 μm), $b^*_{p,1}(\lambda)$ and $b^*_{p,2}(\lambda)$ respectively, as a function of [Chl_a] as:

$$b_p(\lambda) = \left[Chl\_a\right]_1^m\left[b^*_{p,1}(\lambda) - b^*_{p,2}(\lambda)\right]\left[1-\exp\left(-S_1\left[Chl\_a\right]\right)\right] + b^*_{p,2}(\lambda)\left[Chl\_a\right] + b^k_p(\lambda). \quad (13)$$

The spectral dependency of $b^*_{p,1}(\lambda)$, $b^*_{p,2}(\lambda)$ and $b^k_p(\lambda)$, η_1, η_2, and η_k were then estimated using the same procedure which was used for $b_{bp}(\lambda)$ considering that:

$$b_p(\lambda) = b^*_{p,1}(\lambda_0)(\lambda / \lambda_0)^{-\eta_1}\left\{\left[Chl\_a\right]_1^m\left[1-\exp\left(-S_1\left[Chl\_a\right]\right)\right]\right\} + b^*_{p,2}(\lambda_0)(\lambda / \lambda_0)^{-\eta_2}\left\{\left[Chl\_a\right]-\left[Chl\_a\right]_1^m\left[1-\exp\left(-S_1\left[Chl\_a\right]\right)\right]\right\} + b^k_p(\lambda_0)(\lambda / \lambda_0)^{-\eta_k}. \quad (14)$$

Finally, using $b_p(\lambda)$ and $b_{bp}(\lambda)$, the particulate backscattering ratio of the background population, $\tilde{b}^k_{bp}(\lambda)$ and that for the backscattering ratio associated with pico-phytoplankton (<2 μm) and nano-micro-phytoplankton (>2 μm), $\tilde{b}_{bp,1}(\lambda)$ and $\tilde{b}_{bp,2}(\lambda)$ respectively, were calculated as follows:

$$\tilde{b}^k_{bp}(\lambda) = \frac{b^k_{bp}(\lambda)}{b^k_p(\lambda)}, \quad (15)$$

$$\tilde{b}_{bp,1}(\lambda)=\frac{b^*_{bp,1}(\lambda)}{b^*_{p,1}(\lambda)}, \tag{16}$$

$$\tilde{b}_{bp,2}(\lambda)=\frac{b^*_{bp,2}(\lambda)}{b^*_{p,2}(\lambda)}. \tag{17}$$

The associated uncertainties of $\tilde{b}^k_{bp}(\lambda)$, $\tilde{b}_{bp,1}(\lambda)$ and $\tilde{b}_{bp,2}(\lambda)$ were estimated using the standard law of propagation error, such that

$$\frac{\delta\tilde{b}^k_{bp}}{\tilde{b}^k_{bp}}=\sqrt{\left(\frac{\delta b^k_{bp}}{b^k_{bp}}\right)^2+\left(\frac{\delta b^k_{p}}{b^k_{p}}\right)^2}, \tag{18}$$

$$\frac{\delta\tilde{b}_{bp,1}}{\tilde{b}_{bp,1}}=\sqrt{\left(\frac{\delta b^*_{bp,1}}{b^*_{bp,1}}\right)^2+\left(\frac{\delta b^*_{p,1}}{b^*_{p,1}}\right)^2}, \tag{19}$$

$$\frac{\delta\tilde{b}_{bp,2}}{\tilde{b}_{bp,2}}=\sqrt{\left(\frac{\delta b^*_{bp,2}}{b^*_{bp,2}}\right)^2+\left(\frac{\delta b^*_{p,2}}{b^*_{p,2}}\right)^2}. \tag{20}$$

2.9. Statistics

In order to assess how well the model fitted the data, the square of the Pearson correlation coefficient (R^2), the mean absolute difference (MAD) and the root mean square difference (RMSD) were calculated as performance metrics to compare in situ and predicted values of $b_{bp}(\lambda)$ and $b_p(\lambda)$. All the statistical tests were performed in $\log_{10}$ space as we consider that [Chl_a] and the optical properties follows a log normal distribution in the open ocean (Campbell, 1995). The MAD was computed as follows:

$$\mathrm{MAD}=\frac{\sum_{i=1}^{N}\left|X_i^P-X_i^M\right|}{N}. \tag{21}$$

Where N is the number of measurements, X is the variable and the superscripts P and M correspond to the predicted values from the model and the measured in situ values, respectively. The RMSD was computed as follows:

$$\mathrm{RMSD}=\left[\frac{1}{N}\sum_{i=1}^{N}\left(X_i^P-X_i^M\right)^2\right]^{1/2}. \tag{22}$$

3. Results and Discussion

As mentioned above, optical measurements have been collected at 40 stations from surface to 200 m depth and with associated concentrations of [Chl_a] calculated from HPLC measurements or obtained from the calibrated chlorophyll fluorescence using the HPLC measurements. After a quality control applied to the optical measurements, less than 8% of the data collected have been discarded and thus a total of 429 measurements are analyzed here. In this section, the b_{bp}, b_p and $\tilde{b}_{bp}$ relationships with [Chl_a] at 440 nm, 532 nm,

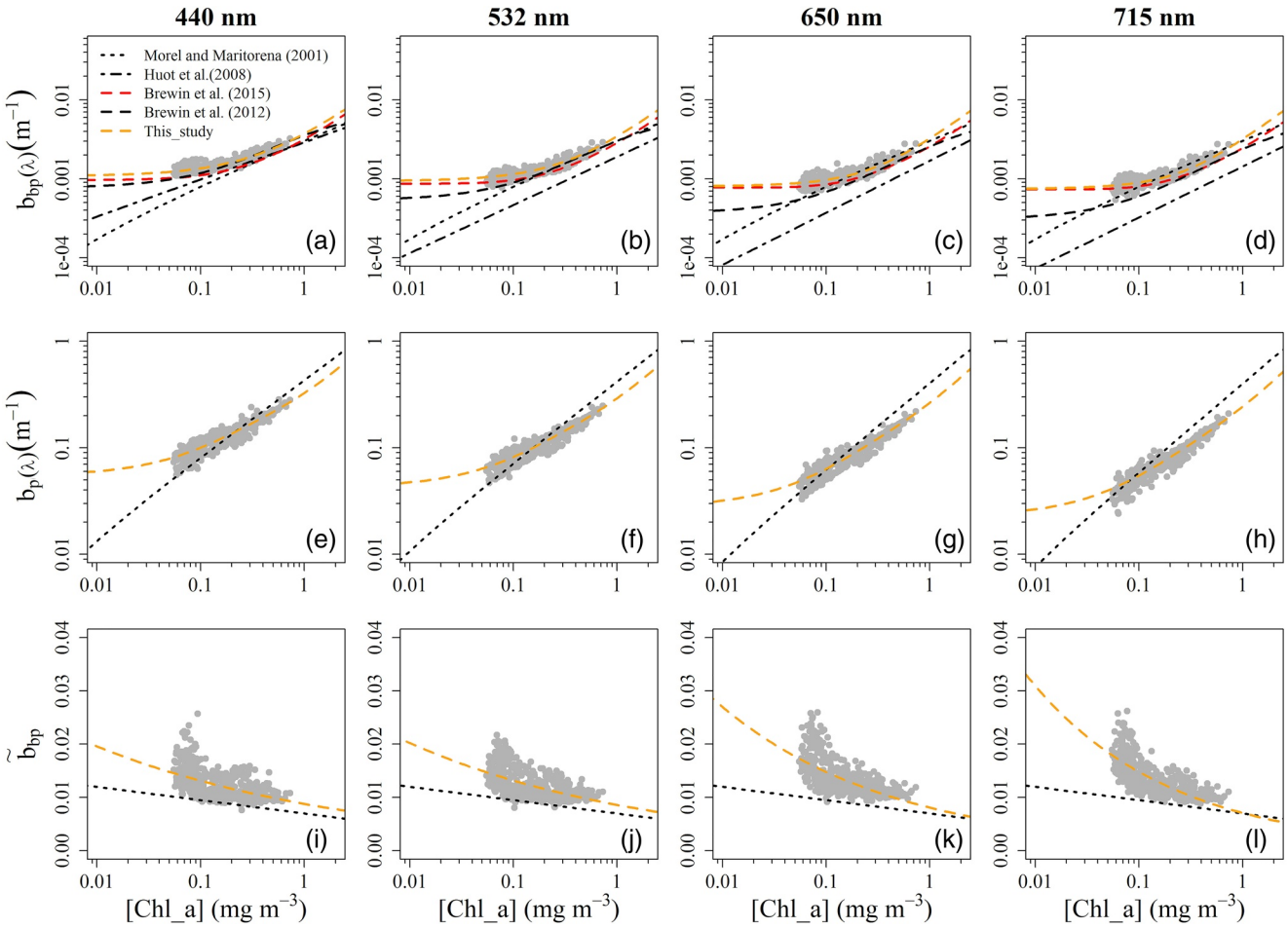

Figure 2. $b_{bp}(\lambda)$ (A-D), $b_p(\lambda)$ (E-H) and $\tilde{b}_{bp}(\lambda)$(I-L) as a function of [Chl_a] at 440 nm, 532 nm, 650 nm and 715 nm with models parameterized to the dataset superimposed.

Table 4
Statistical Results in log_{10} Space (Number of Points [N], Correlation Coefficient [R^2], Root Mean Square Difference [RMSD], and Mean Absolute Difference [MAD]) for the Model Presented in Figure 2

λ	N	R^2	RMSD	MAD	Median ± SD (*Modeled / Measured*)
$b_{bp}(\lambda)$					
440	429	0.85	0.048	0.041	1.03 ± 0.08
532	429	0.84	0.063	0.055	1.06 ± 0.10
650	429	0.81	0.060	0.051	1.04 ± 0.11
715	429	0.83	0.056	0.047	1.03 ± 0.11
$b_p(\lambda)$					
440	429	0.82	0.059	0.047	1.01 ± 0.11
532	429	0.84	0.060	0.046	1.07 ± 0.09
650	429	0.87	0.061	0.047	1.04 ± 0.08
715	429	0.90	0.060	0.045	1.02 ± 0.07

650 nm and 715 nm are presented. Those wavelengths have been chosen to facilitate the comparison with previous studies (Brewin et al., 2015) and to match with those used in various algorithms that are applicable to current ocean color sensors.

Then, we present the spectral dependency of b_{bp}, b_p and $\tilde{b}_{bp}$ of the background population and the chlorophyll-specific populations associated with pico-phytoplankton (<2 μm) and nano/micro-phytoplankton (>2 μm). Finally, we present and discuss our results on $\tilde{b}_{bp}(\lambda)$ as a function of the PSD slope, which are interpreted in the context of refractive index simulations from Twardowski et al. (2001).

3.1. $b_{bp}(\lambda)$, $b_p(\lambda)$ and $\tilde{b}_{bp}(\lambda)$ vs. [Chl_a]

For all wavelengths, $b_{bp}(\lambda)$ increases with increasing [Chl_a], consistent with other studies in various regions. However, it deviates from most global models (existing linear or power law models) with higher values of $b_{bp}(\lambda)$ at low [Chl_a] concentrations (<0.1 mg m^{-3}) (Figures 2a–2c & 2d). For low [Chl_a] concentrations, $b_{bp}(\lambda)$ values vary slightly (Table 3) agreeing with models that considers a background population, such as

Table 5
Comparison of the Model Parameters Used in This Study With Those From Previous studies

Model parameters	This study (440 nm)	Brewin et al., 2015 (443 nm)	Brewin et al., 2012 (470 nm)	Bellacicco et al., 2019 (700 nm)	Zhang et al., 2020 (517 nm)
$b^*_{bp,1}(\lambda)$	0.00274 (0.00235 to 0.00314)	0.0016 (0.0003 to 0.0028)	–	–	–
$b^*_{bp,2}(\lambda)$	0.002618 (0.00246 to 0.00304)	0.0023 (0.0022 to 0.0024)	–	–	–
$b^k_{bp}(\lambda)$	0.001089 (0.001001 to 0.00112)	0.00096 (0.00091 to 0.00102)	0.00070 (0.00065 to 0.00074)	0.00039 (0.00023 to 0.00056)	0.00031 (0.00025 to 0.00043)
γ^1	1.919 (0.834 to 2.943)	4.48 (2.59 to 16.18)	–	–	–
γ^2	−0.106 (−0.098 to −0.115)	0.43 (0.38 to 0.50)	–	–	–
γ^k	0.786 (0.638 to 1.048)	0.54 (0.45 to 0.68)	–	–	–

Note. Values between brackets represent 95% confidence intervals.

that of Brewin et al. (2012, 2015). This is also consistent with the recent study of Zhang et al. (2020) which showed that backscattering by submicron particles in clear ocean waters (<0.1 mg m^{-3} [Chl_a]) is significant, relatively constant, and seems to form a background independent of [Chl_a]. Our re-parameterized model for Red Sea waters adequately captures the general trend of $b_{bp}(\lambda)$ as a function of [Chl_a] (Table 4), especially for low [Chl_a] concentrations whereas the Brewin et al. (2015) model slightly underestimates $b_{bp}(\lambda)$ at higher [Chl_a] concentrations (Figures 2a–2d). These differences are likely explained by: 1) the fact the Brewin et al. (2015) model was not tuned using direct in situ measurements of [Chl_a] and $b_{bp}(\lambda)$; and 2) that the coefficients $\left[Chl\_a\right]_1^m$ and S_1 used in the Brewin et al. (2015) study for pico-phytoplankton were from Brotas et al. (2013). Indeed, Gittings et al. (2019) showed that the coefficients of Brotas et al. (2013), which were derived using HPLC measurements in the Eastern North Atlantic Ocean, contributed to under-estimate the contribution of the pico-phytoplankton population in the Red Sea.

As observed for $b_{bp}(\lambda)$, $b_p(\lambda)$ values increase with increasing [Chl_a] but deviate from the power law model of Morel and Maritorena (2001) at all wavelengths (Figures 2e–2h). Our fit using a three-population scattering model, is seen to capture the general trend of $b_p(\lambda)$ as a function of [Chl_a] (Table 4 and Figures 2e–2h).

The $\tilde{b}_{bp}(\lambda)$ as a function of [Chl_a] exhibits a large variability (Figures 2i–2l) which could be explained by the fact that $b_{bp}(\lambda)$ and $b_p(\lambda)$ are sensitive to different size fractions of particles. The $\tilde{b}_{bp}(\lambda)$ generally decreases with increasing [Chl_a] concentration in agreement with previous studies (Antoine et al., 2011; Loisel et al., 2007; Twardowski et al., 2001; Xi et al., 2015) (Figures 2i–2l). However, our values of $\tilde{b}_{bp}(\lambda)$ are significantly higher than those predicted by the model of Morel and Maritorena (2001) at any given [Chl_a] concentration. This may be due to a higher contribution of non-algal particles or small particles in the Red Sea, relative to other open-ocean environments (Kheireddine et al., 2018). We also found, as reported in previous studies (Twardowski et al., 2001; Whitmire et al., 2007), that $\tilde{b}_{bp}(\lambda)$ does not co-vary well with [Chl_a] for low [Chl_a] concentrations, though we acknowledge measurement uncertainties in $b_{bp}(\lambda)$ and $b_p(\lambda)$ increase at low concentrations, which may reflect on variability in $\tilde{b}_{bp}(\lambda)$. Spectral variations in $\tilde{b}_{bp}(\lambda)$ are not discussed here as they are within the range of measurements uncertainties in $b_{bp}(\lambda)$ and $b_p(\lambda)$ (up to 20%, Boss & Pegau, 2001; Whitmire et al., 2007). At present, there is no consensus regarding $\tilde{b}_{bp}(\lambda)$ spectral behavior. Some studies suggested it is negligible while others found significant changes (Huot et al., 2008; Mckee et al., 2009; Snyder et al., 2008; Whitmire et al., 2007).

3.2. Model Parameters in $b_{bp}(\lambda)$, $b_p(\lambda)$ and $\tilde{b}_{bp}(\lambda)$

We compared our model parameters values with those from previous studies (Table 5) (Brewin et al., 2012, 2015; Bellacicco et al., 2019; Zhang et al., 2020). We first compared our values with those of Brewin

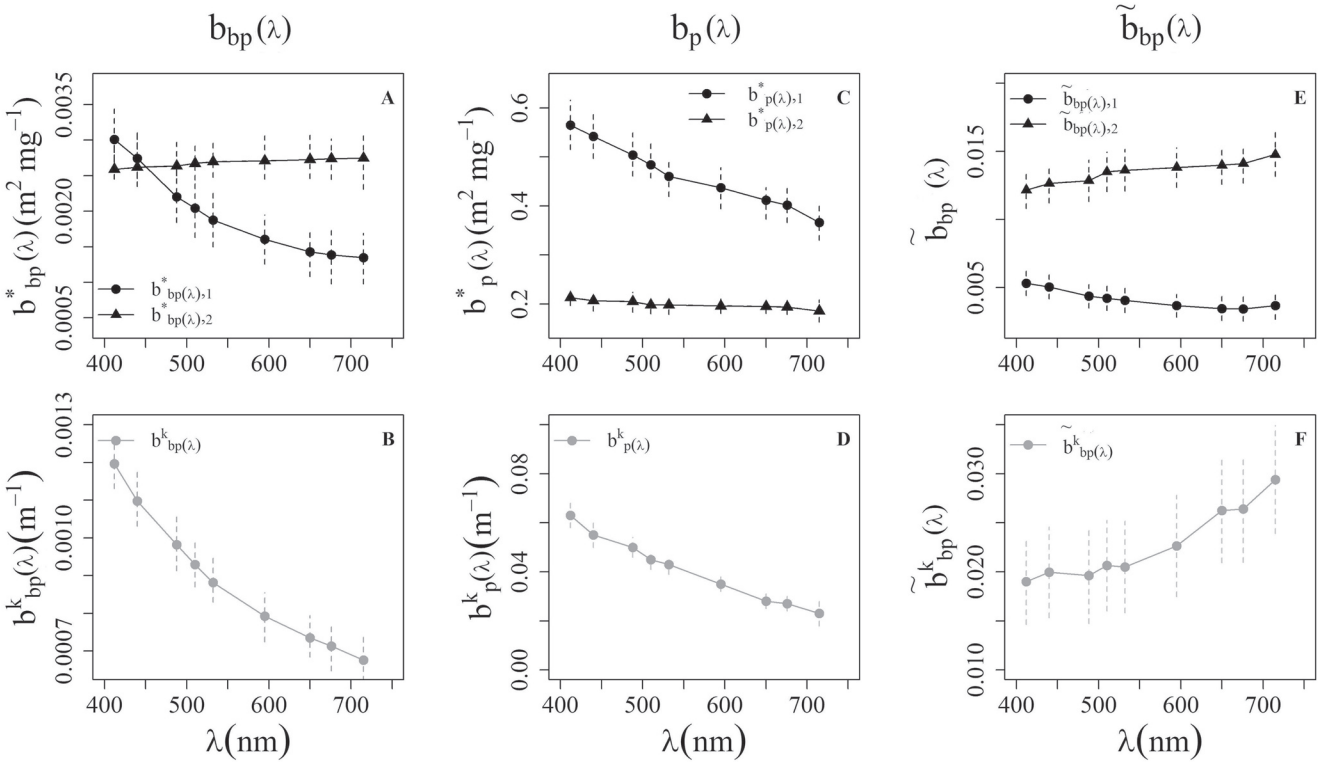

Figure 3. Spectral dependency of each component population to b_{bp} ($b^*_{bp,1}$, $b^*_{bp,2}$ and b^k_{bp}) (A, B), b_p ($b^*_{p,1}$, $b^*_{p,2}$ and b^k_p) (C, D) and $\tilde{b}_{bp}$($\tilde{b}^*_{bp,1}$, $\tilde{b}^*_{bp,2}$ and $\tilde{b}^k_{bp}$) (E, F). The error bars represent the 95% confidence intervals.

et al. (2015) as it is specific to the Red Sea. We found that our $b^*_{bp,1}(443)$ value is within the wide range of values reported in Brewin et al. (2015) whereas, $b^*_{bp,2}(443)$ is significantly higher (beyond the range values reported in Brewin et al. (2015)) which explains the underestimate in $b_{bp}(\lambda)$ at high [Chl_a] using the Brewin et al. (2015) model (Figures 2a–2d). We also noticed that $b^k_{bp}(\lambda)$ is higher from the one in Brewin et al. (2015), though not significantly, with confidence intervals overlapping (Table 5). Our spectral dependency (γ_1 and γ_k) are in the same range or close to those reported in Brewin et al. (2015) whereas the spectral dependency of the nano/micro-phytoplankton population (γ_2) is significantly different. This suggests that the main difference between parameter values in our model and the Brewin et al. (2015) model, is in the population of larger phytoplankton cells due to a higher range of values in $b^*_{bp,2}$ in our study, whereas the range in values in $b^*_{bp,1}$ overlap between both studies (Table 5). The spectral dependency of $b^*_{bp,2}(\lambda)$, γ_2, is close to zero which is consistent with the expectation that larger cells backscatter light similarly at all wavelengths (Kostadinov et al., 2009; Morel, 1987).

When comparing Red Sea $b^k_{bp}(\lambda)$ values with other studies (Table 5), we found that our values are significantly higher than those reported for other areas of the global ocean, acknowledging differences in wavelength (Table 5). Bellacicco et al. (2019) have found that $b^k_{bp}(\lambda)$ varies with region. Such high $b^k_{bp}(\lambda)$ values observed here may be related to the unique conditions in the Red Sea, including its proximity to arid (dusty) terrestrial environments (Prakash et al., 2015; Prospero et al., 2002), and its extreme environmental conditions (among the warmest and most saline seas on the planet) (Chaidez et al., 2017).

The spectral variations and 95% confidence intervals in the three populations for $b_{bp}(\lambda)$, $b_p(\lambda)$ and $\tilde{b}_{bp}(\lambda)$ are presented in Figure 3. First, we observed that the chlorophyll-specific particulate backscattering associated to the nano/micro-phytoplankton's population is mostly higher than those for the pico-phytoplank-

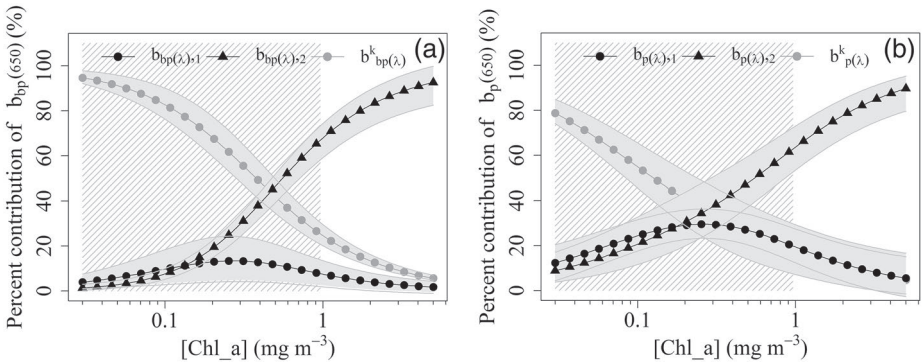

Figure 4. Percent contribution of each component population to $b_{bp}(650)$ (a) and to $b_p(650)$ (b) as a function of [Chl_a] using Equation 12 and Equation 14, respectively. Gray shaded area represent a model ensemble calculated by varying model parameters between 95% confidence intervals (Table 3), in every possible permutation. The gray hatched part represent the range of [Chl_a] concentration observed in Red Sea waters (Kheireddine et al., 2017; Raitsos et al., 2013).

ton's population in agreement with Brewin et al. (2015) whereas, the reverse is observed for particulate scattering (Figures 3a and 3b).

The pattern for particulate scattering is consistent with previous studies that suggested small cells with low internal pigment concentration have a higher chlorophyll-specific scattering coefficient than larger cells with higher internal pigment concentration (Morel, 1987; Kostadinov et al., 2009). However, the higher chlorophyll-specific particulate backscattering associated with the nano/micro-phytoplankton population than for the picoplankton, at green and red wavelengths, is not consistent with previous studies (Morel, 1987; Kostadinov et al., 2009). It is possible that some nano-sized phytoplankton groups that have high backscattering efficiencies like coccolithophores, that have been found in the nearby Mediterranean Sea (D'Amario et al., 2020), are present in Red Sea waters. It is also possible that some of the optical environments where larger cells are present in the Red Sea (i.e., near Coral Reefs) include high concentrations of other covarying constituents, such as detritus, bacteria and viruses, that backscatter light with high efficiency (Ahn et al., 1992). As a result, the pico-phytoplankton population had a significantly lower backscattering ratio than the nano/micro-phytoplankton population (Figure 3c). This may also be related to variations in size and/or composition between both populations (Stramski, 1999; Twardowski et al., 2001; Whitmire et al., 2007). However, theoretical analyses have shown that the shape of the phytoplankton cells could also influence backscattering ratio (Loisel et al., 2007; Whitmire et al., 2007). The backscattering ratio of the background population was higher than for the two phytoplankton populations (Figure 3e) which could be due to differences in the composition of the particulate assemblage, the particulate sizes, structures, and shapes (Boss et al., 2004; Loisel et al., 2007; Twardowski et al., 2001; Ulloa et al., 1994).

The background and pico-phytoplankton populations exhibit steeper spectral slopes than the nano/micro-phytoplankton population for both backscattering and scattering, which is consistent with the assumption that small cells scatter more in the blue region of the spectra in comparison to larger cells, which scatter light similarly at all wavelengths (Kostadinov et al., 2009; Morel, 1987). Note that, as mentioned previously, variability in the spectral variations of $\tilde{b}_{bp}(\lambda)$ are not discussed due to high uncertainties in the backscattering ratio.

The contribution of the background population and the two size classes to $b_{bp}(\lambda)$ and $b_p(\lambda)$ for Red Sea waters are presented in Figures 4a and 4b. For [Chl_a] concentration less than 0.6 mg m^{-3}, $b_{bp}(\lambda)$ is primarily influenced by $b^k_{bp}(\lambda)$ whereas, for [Chl_a] higher than 0.6 mg m^{-3}, $b_{bp}(\lambda)$ is dominated by larger phytoplankton ($b_{bp,2}(\lambda)$) cells (Figure 4a). The contribution of small phytoplankton cells ($b_{bp,1}(\lambda)$) remains low with a maximum contribution of 20% for [Chl_a] values between 0.2 and 0.6 mg m^{-3} (Figure 4a). For [Chl_a] values lower than 0.2 mg m^{-3}, $b_p(\lambda)$ is controlled by the background population whereas, beyond [Chl_a] values of 0.2 mg m^{-3}, $b_p(\lambda)$ is mainly controlled by large phytoplankton cells ($b_{p,2}(\lambda)$) (Figure 4b). As observed with $b_{bp}(\lambda)$, the contribution of small phytoplankton cells ($b_{p,1}(\lambda)$) to $b_p(\lambda)$ is low in general, but higher than the contribution to $b_{bp}(\lambda)$, with a maximum observed value around 25% for [Chl_a]

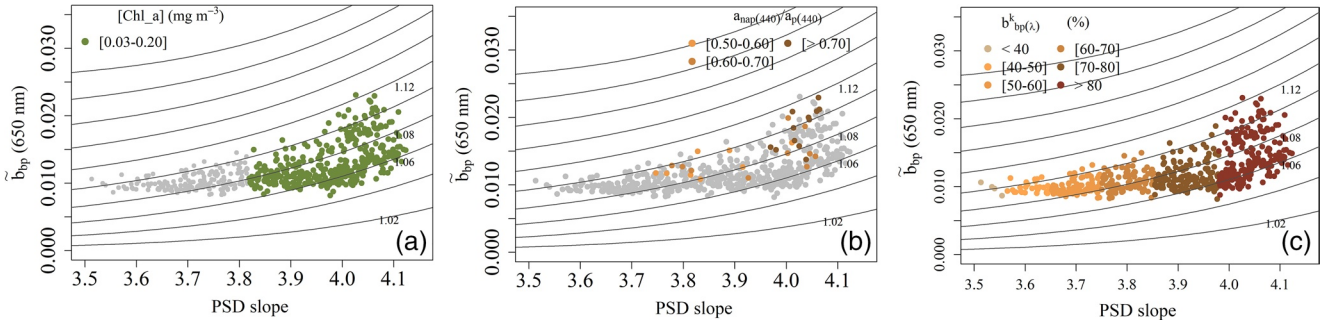

Figure 5. $\tilde{b}_{bp}(\lambda)$ as a function of the PSD slope measurements for [Chl_a] concentration less than to 0.2 mg m-3 (a), $\frac{a_{nap}(440)}{a_p(440)}$ ratio higher than 50% (b) and percent contribution of $b_{bp}^{k}(\lambda)$ to $b_{bp}(\lambda)$ (c) are highlighted. The solid curves overlaid represent the refractive index n contours calculated according to the model of Twardowski et al. (2001).

concentrations between 0.1 and 0.8 mg m^{-3}. Thus, $b_{bp}(\lambda)$ and $b_p(\lambda)$ are mainly driven by the background population for [Chl_a] concentrations lower than 0.2 $mg.m^{-3}$.

3.3. Refractive Index of the Background Population ($b_{bp}^{k}(\lambda)$ and $b_p^{k}(\lambda)$)

To attempt to characterize the composition of the particulate assemblage for the background population, we used the analytical model of Twardowski (2001). This consists of simulations of the refractive index (n) from $\tilde{b}_{bp}(\lambda)$ and the PSD (Figure 5). Most of the PSD slope ranged from 3.8 to 4.1 for [Chl_a] concentrations less than 0.2 mg m^{-3} (Figure 5a), which is in agreement with expected values for oligotrophic oceans (Antoine et al., 2011; Kostadinov et al., 2009; Organelli et al., 2020) compared to those expected for coastal and other highly-productivity areas (Loisel et al., 2007; White et al., 2015; Xi et al., 2014). Indeed, previous studies showed that oligotrophic regions of the world ocean are associated with the predominance of small phytoplankton, whereas productive, high-nutrient regions are associated with large cells (Kostadinov et al., 2009; Loisel et al., 2007; Organelli et al., 2020; Xi et al., 2014). This suggests that a high proportion of small sized particles dominate the Red Sea, in agreement with previous studies (Brewin et al., 2015; Kheireddine et al., 2017, 2018). The range of variability in n (1.04–1.12) is within the same range reported in other areas of the global ocean (Antoine et al., 2011; Loisel et al., 2007; Twardowski et al., 2001; Xi et al., 2015) (Figure 5). As expected, Red Sea waters are characterized by a mixture of particles with different sizes and composition. It has been suggested that some non-algal particles (inorganic and organic) have a refractive index varying between 1.04 and 1.26 whereas, phytoplankton cells have a lower refractive index (1.02–1.092) due to their high water content (Aas, 1996; Poulin et al., 2018; Stramski, 1999; Twardowski et al., 2001; Wozniak & Stramski, 2004). We also found that samples with PSD slopes higher than 3.9 are associated to low values of [Chl_a] and to high values in the ratio of $a_{nap}(\lambda)$ to $a_p(\lambda)$ at 440 nm ($\frac{a_{nap}(440)}{a_p(440)}$) (Figures 5a and 5b) indicating the presence of a large amount of small non-algal particles. This is consistent with the trend observed between [Chl_a] and $\frac{a_{nap}(440)}{a_p(440)}$ where the contribution of non-algal particles decrease with higher [Chl_a] concentrations associated to a predominance of large particles (Figures 6a and 6b).

Several studies showed that the Red Sea is experiencing regular inputs from dust (Ginoux et al., 2012; Prakash et al., 2015; Prospero et al., 2002) which could partly explain the high $\frac{a_{nap}(440)}{a_p(440)}$ values. Several studies also demonstrated that warm water temperature can have a positive effect on the growth of bacteria, which can influence particle characteristics in the Red Sea (Kirchman et al., 2005; Lekunberri et al., 2010; Lopez-Urrutia et al., 2006; Morales-Baquero et al., 2013; Reche et al., 2009; Sarmento et al., 2010) and thus $\frac{a_{nap}(440)}{a_p(440)}$ values.

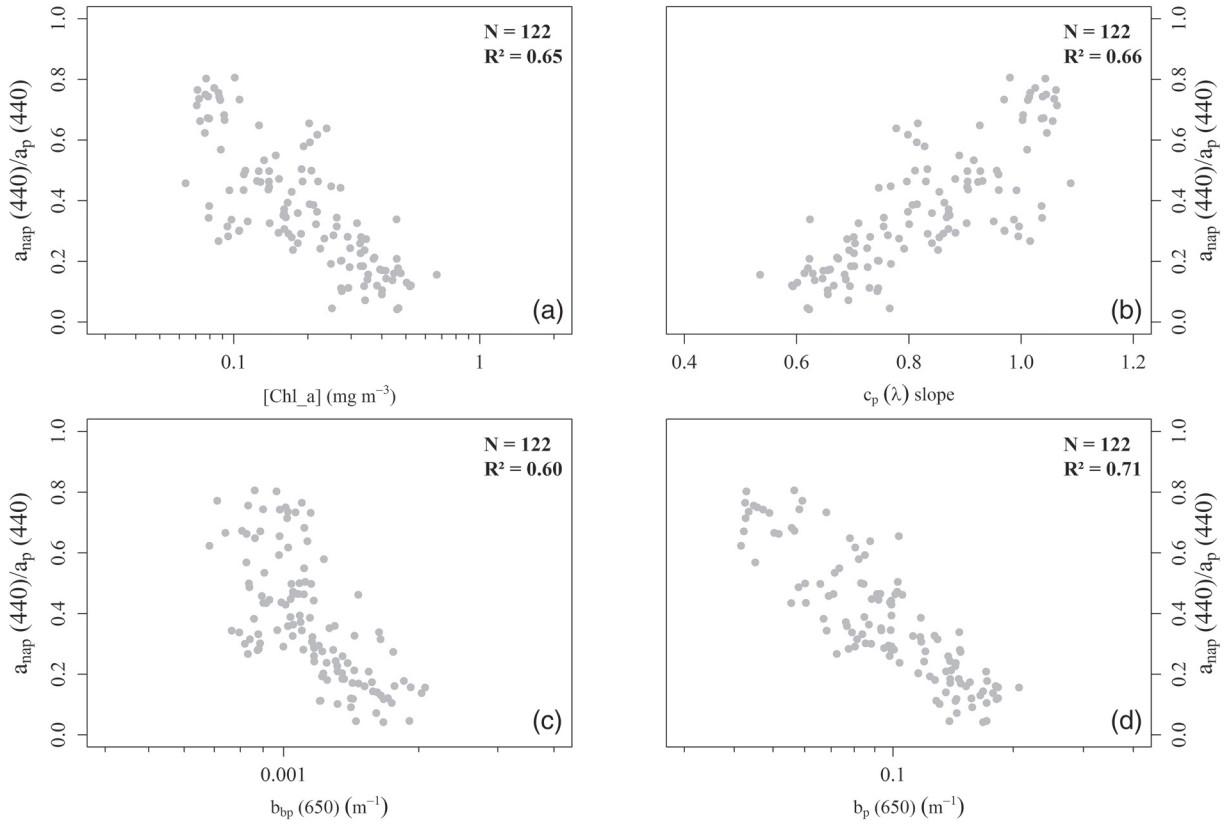

Figure 6. $\frac{a_{nap}(440)}{a_p(440)}$ ratio as a function of [Chl_a] (a), $c_p(\lambda)$ slope (b), $b_{bp}(650)$ (c) and $b_p(650)$ (d).

Furthermore, we would also expect to see that high proportions of non-algal particles might be associated to a higher contribution of the background population in $b_{bp}(\lambda)$. While few measurements have been collected, this is consistent with our results (Figures 5b and 5c). We observe a relationship between the background population ($b_{bp}^k(\lambda)$ values) and the amount of non-algal particles ($\frac{a_{nap}(440)}{a_p(440)}$ values), where $\frac{a_{nap}(440)}{a_p(440)}$ values increase with increases in $b_{bp}^k(\lambda)$ values (Figures 5b and 5c). Indeed, the analysis of n and $\frac{a_{nap}(440)}{a_p(440)}$ values suggest that the background population ($b_{bp}^k(\lambda)$ and $b_p^k(\lambda)$) is likely dominated by small non-algal particles (bacteria, dusts), as shown by high $\tilde{b}_{bp}(\lambda)$ values associated to low [Chl_a] concentrations and high $\frac{a_{nap}(440)}{a_p(440)}$ (Figures 5a–5c).

This is also consistent with the relationship of $\frac{a_{nap}(440)}{a_p(440)}$ with $b_{bp}(650)$ and $b_p(650)$ (Figures 6c and 6d). We observed that $b_{bp}(650)$ and $b_p(650)$ are significantly inversely correlated with $\frac{a_{nap}(440)}{a_p(440)}$ (Figures 6c and 6d). Low $\frac{a_{nap}(440)}{a_p(440)}$ ratio is indicative of large amount of phytoplankton and is consistent with high $b_{bp}(650)$ and $b_p(650)$ values (Figures 6c and 6d) whereas high $\frac{a_{nap}(440)}{a_p(440)}$ ratio is indicative of a large amount of non-algal particles associated to low $b_{bp}(650)$ values (Figure 6c).

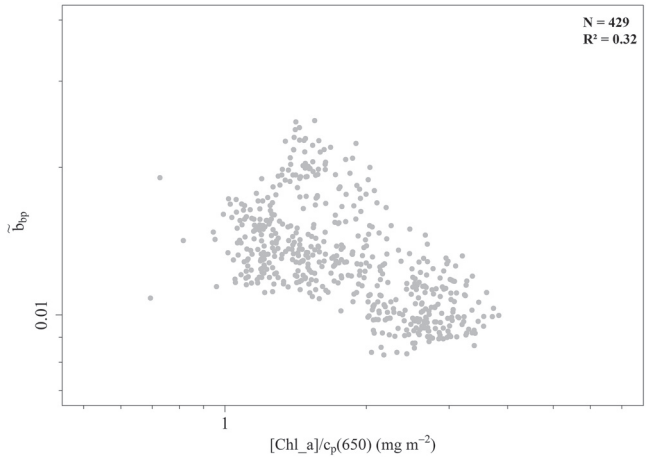

Figure 7. $\tilde{b}_{bp}(650)$ as a function of the ratio of [Chl_a] to c_p (650).

While no direct measurements of n have been used here, we can speculate that some of the non-algal particles comprise in the background population may have a higher refractive index than those for the phytoplankton population. Whether this is unique to the Red Sea, or also characteristic of other oceans, remains to be seen, and further work is needed to verify this speculation. In view of this, we also analyzed the relationship between $\tilde{b}_{bp}(650)$ and the ratio of [Chl_a] to $c_p(650)$, a proxy for the relative proportion of phytoplankton within the total particulate matter (Boss et al., 2004; Loisel et al., 2007) (Figure 7). While the relation is poor ($R^2 = 0.32$), we observed a negative correlation between these two parameters in agreement with Boss et al. (2004), showing that a relatively low proportion of phytoplankton to total particulate matter (i.e., low $\frac{[Chl\_a]}{c_{p(650)}}$ ratio) is associated with high $\tilde{b}_{bp}(650)$ values (i.e., higher n) (Figure 7).

Given that $b_{bp}^{k}(\lambda)$ and $b_{p}^{k}(\lambda)$ dominates at low [Chl_a] concentration (less than 0.2 mg m^{-3}) and considering that the Red Sea is mainly considered as an oligotrophic basin (Kheireddine et al., 2017; Raitsos et al., 2013), this suggests that Red Sea $b_{bp}(\lambda)$ and $b_p(\lambda)$ measurements are strongly influenced by a background population of non-algal particles.

4. Potential Biases in This Study

In this study, $b_{bp}(\lambda)$, $b_p(\lambda)$ and $c_p(\lambda)$ measurements have been inferred from different sensors having different pathlengths and acceptance angles, which could lead to additional uncertainties in $\tilde{b}_{bp}(\lambda)$ values (Boss & Pegau, 2001; Boss et al., 2009; Whitmire et al., 2007). Furthermore, as $b_{bp}(\lambda)$ and $b_p(\lambda)$ measurements are estimated in different ways ($b_p(\lambda)$ derived from an ac-s sensor having removed the contribution from 0.2 micron seawater), they may represent slightly different particle pools which could induce biases in our scattering measurements. Indeed, Zhang et al. (2020) showed that backscattering by particles less than 0.2 micron, in clear ocean waters is significant and independent of the backscattering by larger particles. This could also lead to additional uncertainties on our interpretation of $\tilde{b}_{bp}(\lambda)$. Nevertheless, Dall'Olmo et al. (2009, 2012) have showed that differences between $b_{bp}(\lambda)$ filtered measurements (i.e., >0.2 μm) and those not filtered (i.e., all particles) are within the uncertainties of the measurements.

The model of Twardowski et al. (2001), using $\tilde{b}_{bp}(\lambda)$ and PSD slope (i.e., predicted from $c_p(\lambda)$ slope) to infer the refractive index of the particle assemblage, is based on Mie theory, which underlies several assumptions such that marine particles are spherical and homogeneous and follow a Junge-type size distribution. Such assumptions may contribute to errors in the refractive index values presented here (Kitchen & Zaneveld, 1992; Organelli et al., 2018; Poulin et al., 2018). Indeed, recent studies (Organelli et al., 2018; Poulin et al., 2018) have confirmed that coated sphere models, that consider the structural complexity of marine particles, are capable of reproducing measured $b_{bp}(\lambda)$ in the ocean without making assumptions on the presence of sub-micron particles. However, despite the potential issues presented here, the model of Twardowski et al. (2001) has been shown to be robust to particles with different composition (i.e., refractive index) in various area of the global ocean, in cases where no in situ data of refractive index is available (Antoine et al., 2011; Boss et al., 2001; Loisel et al., 2007; Sun et al., 2019; Xi et al., 2015). Owing to the limitations mentioned above, the results presented here must be interpreted with an element of caution, and more work is needed.

5. Conclusion

Using a unique optical dataset collected in the Red Sea, we relate the backscattering coefficient to changes in [Chl_a] using a conceptual model that partitions particles into three components, a background component, and two other components representative of environments dominated by small (<2 μm) and larger

plankton (>2 μm). We then extend the approach, for the first time, to modeling of total scattering, allowing the analysis of the backscattering ratio for each component in the model. We find the backscattering ratio of the background component to be significantly higher than the two phytoplankton-influenced components. Further analysis using optical measurements of algal and non-algal particle absorption, the spectral slope of the beam attenuation of particles, and refractive index simulations, suggest that the background population ($b_{bp}^{k}(\lambda)$) is likely dominated by a pool of small non-algal particles, consistent with the assumptions made by Bellacicco et al. (2019). Thus, our results suggest that $b_{bp}(\lambda)$ is strongly influenced by a background population of non-algal particles for [Chl_a] less than 0.2 mg m^{-3} in Red Sea waters. To improve our interpretation of $b_{bp}(\lambda)$ and $b_{p}(\lambda)$ further, future efforts should focus on improving our understanding of the nature and composition of particles that make up this background population. Our work supports the combination of conceptual models and optical measurements for studying marine biogeochemical processes, and has implications for developing satellite ocean-color algorithms for the region. Indeed, understanding the sources of $b_{bp}(\lambda)$ in order to feasibly detect different pool of particles from ocean-color remote sensing will improve estimates of fundamental biogeochemical variables such as [Chl_a], particulate organic carbon and phytoplankton functional types (size and community structure) which will then improve our understanding of marine biogeochemical cycling.

Data Availability Statement

The data presented in this study are archived in KAUST repository (https://doi.org/10.25781/KAUST-PSDX7).

Acknowledgments
The authors express their gratitude to the scientists, officers and crews of the research vessel Thuwal and also the Coastal and Marine Resources Core Lab for logistical support and assistance onboard during the fieldwork. U. Langner is cordially thanked for plotting the map of the Red Sea. We also cordially thanked Xiaodong Zhang and the two other anonymous reviewers for their valuable constructive comments that helped to improve our manuscript. This study is funded by the King Abdullah University of Science and Technology (KAUST), Kingdom of Saudi Arabia. RJWB was supported by the European Space Agency (ESA) project "Biological Pump and Carbon Exchange Processes (BICEP)", and by the Simons Foundation Project "Collaboration on Computational Biogeochemical Modeling of Marine Ecosystems (CBIOMES)" (549947, SS).

References

Aas, E. (1996). Refractive index of phytoplankton derived from its metabolite composition. *Journal of Plankton Research*, *18*(12), 2223–2249. https://doi.org/10.1093/plankt/18.12.2223

Ahn, Y. H., Bricaud, A., & Morel, A. (1992). Light backscattering efficiency and related properties of some phytoplankters. *Deep-Sea Research A-Oceanographic Research Papers*, *39*(11–12A), 1835–1855. https://doi.org/10.1016/0198-0149(92)90002-b

Al-Taani, A. A., Rashdan, M., & Khashashneh, S. (2015). Atmospheric dry deposition of mineral dust to the Gulf of Aqaba, Red Sea: Rate and trace elements. *Marine Pollution Bulletin*, *92*(1–2), 252–258. https://doi.org/10.1016/j.marpolbul.2014.11.047

Antoine, D., Siegel, D. A., Kostadinov, T., Maritorena, S., Nelson, N. B., Gentili, B., et al. (2011). Variability in optical particle backscattering in contrasting bio-optical oceanic regimes. *Limnology & Oceanography*, *56*(3), 955–973. https://doi.org/10.4319/lo.2011.56.3.0955

Baars, M., Schalk, P., & Veldhuis, M. (1998). Seasonal fluctuations in plankton biomass and productivity in the ecosystems of the Somali Current, Gulf of Aden, and Southern Red Sea. In K. Sherman, E. Okemwa, & M. Ntiba, Eds., *Large marine ecosystems of the Indian Ocean: Assessment, sustainability, and management* (p. 394). Cambridge, MA: Blackwell Science, Inc.

Behrenfeld, M. J., Boss, E., Siegel, D. A., & Shea, D. M. (2005). Carbon-based ocean productivity and phytoplankton physiology from space. *Global Biogeochemical Cycles*, *19*(1). https://doi.org/10.1029/2004gb002299

Belkin, I. M. (2009). Rapid warming of Large Marine Ecosystems. *Progress in Oceanography*, *81*(1–4), 207–213. https://doi.org/10.1016/j.pocean.2009.04.011

Bellacicco, M., Cornec, M., Organelli, E., Brewin, R. J. W., Neukermans, G., Volpe, G., et al. (2019). Global variability of optical backscattering by non-algal particles from a biogeochemical-argo data set. *Geophysical Research Letters*, *46*(16), 9767–9776. https://doi.org/10.1029/2019gl084078

Bishop, J. K. B., Davis, R. E., & Sherman, J. T. (2002). Robotic observations of dust storm enhancement of carbon biomass in the North Pacific. *Science*, *298*(5594), 817–821. https://doi.org/10.1126/science.1074961

Boss, E., & Pegau, W. S. (2001). Relationship of light scattering at an angle in the backward direction to the backscattering coefficient. *Applied Optics*, *40*, 5503–5505.

Boss, E., Pegau, W. S., Lee, M., Twardowski, M., Shybanov, E., Korotaev, G., & Baratange, F. (2004). Particulate backscattering ratio at LEO 15 and its use to study particle composition and distribution. *Journal of Geophysical Research*, *109*, C01014. https://doi.org/10.1029/2002JC001514

Boss, E., Twardowski, M. S., & Herring, S. (2001). Shape of the particulate beam attenuation spectrum and its inversion to obtain the shape of the particulate size distribution. *Applied Optics*, *40*(27), 4885–4893. https://doi.org/10.1364/ao.40.004885

Boss, E., Wayne, S. H., Behrenfeld, M., & Dall'Olmo, G. (2009). Acceptance angle effects on the beam attenuation in the ocean. *Optics Express*, *17*, 1535–1550. https://doi.org/10.1364/OE.17.001535

Boyd, P. W., Claustre, H., Levy, M., Siegel, D. A., & Weber, T. (2019). Multi-faceted particle pumps drive carbon sequestration in the ocean. *Nature*, *568*(7752), 327–335. https://doi.org/10.1038/s41586-019-1098-2

Breitburg, D., Levin, L. A., Oschlies, A., Grégoire, M., Chavez, F. P., Conley, D. J., et al. (2018). Declining oxygen in the global ocean and coastal waters. *Science*, *359*(6371), 46–+. https://doi.org/10.1126/science.aam7240

Brewin, R. J. W., Dall'Olmo, G., Sathyendranath, S., & Hardman-Mountford, N. J. (2012). Particle backscattering as a function of chlorophyll and phytoplankton size structure in the open-ocean. *Optics Express*, *20*(16), 17632–17652. https://doi.org/10.1364/oe.20.017632

Brewin, R. J. W., Raitsos, D. E., Dall'Olmo, G., Zarokanellos, N., Jackson, T., Racault, M. F., et al. (2015). Regional ocean-color chlorophyll algorithms for the Red Sea. *Remote Sensing of Environment*, *165*, 64–85. https://doi.org/10.1016/j.rse.2015.04.024

Bricaud, A., & Stramski, D. (1990). Spectral absorption coefficients of living phytoplankton and non-algal biogenous matter: A comparison between the Peru upwelling are and the Sargasso Sea. *Limnology & Oceanography*, *35*(3), 562–582. https://doi.org/10.4319/lo.1990.35.3.0562

Briggs, N., G. Dall'Olmo, & H. Claustre (2020). Major role of particle fragmentation in regulating biological sequestration of CO2 by the oceans, *Science*, *367*(6479), 791–793. https://doi.org/10.1126/science.aay1790

Briggs, N., Perry, M. J., Cetinic, I., Lee, C., D'Asaro, E., Gray, A. M., & Rehm, E. (2011). High-resolution observations of aggregate flux during a sub-polar North Atlantic spring bloom. *Deep-Sea Research Part I-Oceanographic Research Papers*, *58*(10), 1031–1039. https://doi.org/10.1016/j.dsr.2011.07.007

Brotas, V., Brewin, R. J. W., Sá, C., Brito, A. C., Silva, A., Mendes, C. R., et al. (2013). Deriving phytoplankton size classes from satellite data: Validation along a trophic gradient in the eastern Atlantic Ocean. *Remote Sensing of Environment*, *134*, 66–77. https://doi.org/10.1016/j.rse.2013.02.013

Campbell, J. W. (1995). The lognormal distribution as a model for bio-optical variability in the sea. *Journal of Geophysical Research*, *100*(C7), 13237–13254. https://doi.org/10.1029/95jc00458

Chaidez, V., Dreano, D., Agusti, S., Duarte, C. M., & Hoteit, I. (2017). Decadal trends in Red Sea maximum surface temperature. *Scientific Reports*, *7*. https://doi.org/10.1038/s41598-017-08146-z

Dall'Olmo, G., Boss, E., Behrenfeld, M. J., & Westberry, T. K. (2012). Particulate optical scattering coefficients along an Atlantic Meridional Transect. *Optics Express*, *20*(19), 21532–21551. https://doi.org/10.1364/oe.20.021532

Dall'Olmo, G., & Mork, K. A. (2014). Carbon export by small particles in the Norwegian Sea. *Geophysical Research Letters*, *41*(8), 2921–2927. https://doi.org/10.1002/2014gl059244

Dall'Olmo, G., Dingle, J., Polimene, L., Brewin, R. J. W., & Claustre, H. (2016), Substantial energy input to the mesopelagic ecosystem from the seasonal mixed-layer pump, *Nature Geoscience*, *9*(11), 820–823. https://doi.org/10.1038/ngeo2818

Dall'Olmo, G., Westberry, T. K., Behrenfeld, M. J., Boss, E., & Slade, W. H. (2009). Significant contribution of large particles to optical backscattering in the open ocean. *Biogeosciences*, *6*, 947–967. https://doi.org/10.5194/bg-6-947-2009

D'Amario, B. C., Pérez, M., Grelaud, P., Pitta, E., Kradakopoulou, & Ziveri, P. (2020). Coccolithophore community response to ocean acidification and warming in the Eastern Mediterranean Sea: Results from a mesocosm experiment. *Scientific Reports*, *10*, 12637. https://doi.org/10.1038/s41598-020-69519-5

Estapa, M., Durkin, C., Buesseler, K., Johnson, R., & Feen, M. (2017). Carbon flux from bio-optical profiling floats: Calibrating transmissometers for use as optical sediment traps. *Deep-Sea Research Part I-Oceanographic Research Papers*, *120*, 100–111. https://doi.org/10.1016/j.dsr.2016.12.003

Estapa, M. L., Feen, M. L., & Breves, E. (2019). Direct observations of biological carbon export from profiling rituals in the subtropical North Atlantic. *Global Biogeochemical Cycles*, *33*(3), 282–300. https://doi.org/10.1029/2018gb006098

Ginoux, P., Prospero, J. M., Gill, T. E., Hsu, N. C., & Zhao, M. (2012). Global-scale attribution of anthropogenic and natural dust sources and their emission rates based on MODIS deep blue aerosol products. *Reviews of Geophysics*, *50*. https://doi.org/10.1029/2012rg000388

Gittings, J. A., Brewin, R. J. W., Raitsos, D. E., Kheireddine, M., Ouhssain, M., Jones, B. H., et al. (2019). Remotely sensing phytoplankton size structure in the Red Sea. *Remote Sensing of Environment*, *234*. https://doi.org/10.1016/j.rse.2019.111387

Huot, Y., Morel, A., Twardowski, M. S., Stramski, D., & Reynolds, R. A. (2008). Particle optical backscattering along a chlorophyll gradient in the upper layer of the eastern South Pacific Ocean. *Biogeosciences*, *5*(2), 495–507. https://doi.org/10.5194/bg-5-495-2008

Kheireddine, M., & Antoine, D. (2014). Diel variability of the beam attenuation and backscattering coefficients in the northwestern Mediterranean Sea (BOUSSOLE site). *Journal of Geophysical Research: Oceans*, *119*, 5465–5482. https://doi.org/10.1002/2014JC010007

Kheireddine, M., Dall'Olmo, G., Ouhssain, M., Krokos, G., Claustre, H., Schmechtig, C., et al. (2020). Organic carbon export and loss rates in the Red Sea. *Global Biogeochemical Cycles*, *34*, e2020GB006650. https://doi.org/10.1029/2020GB006650

Kheireddine, M., Ouhssain, M., Claustre, H., Uitz, J., Gentili, B., & Jones, B. H. (2017). Assessing pigment-based phytoplankton community cistributions in the Red Sea. *Frontiers in Marine Science*, *4*. https://doi.org/10.3389/fmars.2017.00132

Kheireddine, M., Ouhssain, M., Organelli, E., Bricaud, A., & Jones, B. H. (2018). Light absorption by suspended particles in the Red Sea: Effect of phytoplankton community size structure and pigment Ccmposition. *Journal of Geophysical Research: Oceans*, *123*(2), 902–921. https://doi.org/10.1002/2017jc013279

Kirchman, D. L., Malmstrom, R. R., & Cottrell, M. T. (2005). Control of bacterial growth by temperature and organic matter in the Western Arctic. *Deep-Sea Research Part Ii-Topical Studies in Oceanography*, *52*(24–26), 3386–3395. https://doi.org/10.1016/j.dsr2.2005.09.005

Kishino, M., Takahashi, M., Okami, N., & Ichimura, S. (1985). Estimation of the spectral absorption coefficients phytoplankton in the sea. *Bulletin of Marine Science*, *37*(2), 634–642.

Kitchen, J. C., & Zaneveld, J. R. V. (1992). A three-layered sphere model of the optical properties of phytoplankton. *Limnology & Oceanography*, *37*, 1680–1690. https://doi.org/10.4319/lo.1992.37.8.1680

Koestner, D., Stramski, D., & Reynolds, R. A. (2018). Measurements of the volume scattering function and the degree of linear polarization of light scattered by contrasting natural assemblages of marine particles. *Applied Sciences*, *8*, 2690. https://doi.org/10.3390/app8122690

Kostadinov, T. S., Siegel, D. A., & Maritorena, S. (2009). Retrieval of the particle size distribution from satellite ocean color observations. *Journal of Geophysical Research*, *114*. https://doi.org/10.1029/2009jc005303

Kwon, E. Y., Primeau, F., & Sarmiento, J. L. (2009). The impact of remineralization depth on the air-sea carbon balance. *Nature Geoscience*, *2*(9), 630–635. https://doi.org/10.1038/ngeo612

Lekunberri, I., Lefort, T., Romero, E., Vazquez-Dominguez, E., Romera-Castillo, C., Marrase, C., et al. (2010). Effects of a dust deposition event on coastal marine microbial abundance and activity, bacterial community structure and ecosystem function. *Journal of Plankton Research*, *32*(4), 381–396. https://doi.org/10.1093/plankt/fbp137

Loisel, H., Meriaux, X., Berthon, J. F., & Poteau, A. (2007). Investigation of the optical backscattering to scattering ratio of marine particles in relation to their biogeochemical composition in the eastern English Channel and southern North Sea. *Limnology & Oceanography*, *52*(2), 739–752. https://doi.org/10.4319/lo.2007.52.2.0739

Lopez-Urrutia, A., San Martin, E., Harris, R. P., & Irigoien, X. (2006). Scaling the metabolic balance of the oceans. *Proceedings of the National Academy of Sciences of the United States of America*, *103*(23), 8739–8744. https://doi.org/10.1073/pnas.0601137103

Marañón, E. (2019). Phytoplankton size structure. In J. K. Cochran, H. J. Bokuniewicz, & P. L. Yager (Eds.), *Encyclopedia of ocean sciences* (3rd ed.). Oxford: Academic Press.

McKee, D., Chami, M., Brown, I., Calzado, V. S., Doxaran, D., & Cunningham, A. (2009). Role of measurement uncertainties in observed variability in the spectral backscattering ratio: A case study in mineral-richcoastal waters. *Applied Optics*, *48*, 4663–4675. https://doi.org/10.1364/AO.48.004663

Mitchell, B. G., Kahru, M., Wieland, J., & Stramska, M. (2003). Determination of spectral absorption coefficients of particles, dissolved material and phytoplankton for discrete water samples. In J. L. Mueller, G. S. Fargion, & C. R. McClain (Eds.), *Ocean optics protocols for satellite ocean color sensor validation, revision 4, volume IV: Inherent optical properties: Instruments, characterizations, field measurements and data analysis protocols*. Greenbelt, MD: NASA.

Morales-Baquero, R., Pulido-Villena, E., & Reche, I. (2013). Chemical signature of Saharan dust on dry and wet atmospheric deposition in the south-western Mediterranean region. *Tellus Series B Chemical and Physical Meteorology*, *65*. https://doi.org/10.3402/tellusb.v65i0.18720

Morel, A. (1987). Chlorophyll specific scattering coefficient of phytoplankton: A simplified theoretical approach. *Deep-Sea Research Part A-Oceanographic Research Papers*, *34*(7), 1093–1105. https://doi.org/10.1016/0198-0149(87)90066-5

Morel, A., & Maritorena, S. (2001). Bio-optical properties of oceanic waters: A reappraisal. *Journal of Geophysical Research-Oceans*, *106*(C4), 7163–7180. https://doi.org/10.1029/2000jc000319

Morel, A., & Yu-Hwan, A. (1991). Optics of heterotrophic nanoflagellates and ciliates: A tentative assessment of their scattering role in oceanic waters compared to those of bacterial and algal cells. *Journal of Marine Research*, *49*, 177–202.

Organelli, E., Barbieux, M., Claustre, H., Schmechtig, C., Poteau, A., Bricaud, A., et al. (2017). Two databases derived from BGC-Argo float measurements for marine biogeochemical and bio-optical applications. *Earth System Science Data*, *9*(2), 861–880. https://doi.org/10.5194/essd-9-861-2017

Organelli, E., Bricaud, A., Antoine, D., & Uitz, J. (2013). Multivariate approach for the retrieval of phytoplankton size structure from measured light absorption spectra in the Mediterranean Sea (BOUSSOLE site). *Applied Optics*, *52*(11), 2257–2273. https://doi.org/10.1364/AO.52.002257

Organelli, E., Dall'Olmo, G., Brewin, R. J., Nencioli, F., & Tarran, G. A. (2020). Drivers of spectral optical scattering by particles in the upper 500 m of the Atlantic Ocean. *Optics Express*, *28*, 34147–34166. https://doi.org/10.1364/OE.408439

Organelli, E., Dall'Olmo, G., Brewin, R. J. W., Tarran, G. A., Boss, E., & Bricaud, A. (2018). The open-ocean missing backscattering is in the structural complexity of particles. *Nature Communications*, *9*, 5439. https://doi.org/10.1038/s41467-018078146

Poulin, C., Zhang, X. D., Yang, P., & Huot, Y. (2018). Diel variations of the attenuation, backscattering and absorption coefficients of four phytoplankton species and comparison with spherical, coated spherical and hexahedral particle optical models. *Journal of Quantitative Spectroscopy & Radiative Transfer*, *217*, 288–304. https://doi.org/10.1016/j.jqsrt.2018.05.035

Prakash, P. J., Stenchikov, G., Kalenderski, S., Osipov, S., & Bangalath, H. (2015). The impact of dust storms on the Arabian Peninsula and the Red Sea. *Atmospheric Chemistry and Physics*, *15*(1), 199–222. https://doi.org/10.5194/acp-15-199-2015

Prospero, J. M., Ginoux, P., Torres, O., Nicholson, S. E., & Gill, T. E. (2002). Environmental characterization of global sources of atmospheric soil dust identified with the Nimbus 7 Total Ozone Mapping Spectrometer (TOMS) absorbing aerosol product. *Reviews of Geophysics*, *40*(1). https://doi.org/10.1029/2000rg000095

Raitsos, D. E., Pradhan, Y., Brewin, R. J. W., Stenchikov, G., & Hoteit, I. (2013). Remote Sensing the Phytoplankton Seasonal Succession of the Red Sea. *PloS One*, *8*(6). https://doi.org/10.1371/journal.pone.0064909

Ras, J., Claustre, H., & Uitz, J. (2008). Spatial variability of phytoplankton pigment distributions in the Subtropical South Pacific Ocean: comparison between in situ and predicted data. *Biogeosciences*, *5*(2), 353–369. https://doi.org/10.5194/bg-5-353-2008

Reche, I., Ortega-Retuerta, E., Romera, O., Pulido-Villena, E., Morales-Baquero, R., & Casamayor, E. O. (2009). Effect of Saharan dust inputs on bacterial activity and community composition in Mediterranean lakes and reservoirs. *Limnology & Oceanography*, *54*(3), 869–879. https://doi.org/10.4319/lo.2009.54.3.0869

Sarmento, H., Montoya, J. M., Vazquez-Dominguez, E., Vaque, D., & Gasol, J. M. (2010). Warming effects on marine microbial food web processes: How far can we go when it comes to predictions? *Philosophical Transactions of the Royal Society B: Biological Sciences*, *365*(1549), 2137–2149. https://doi.org/10.1098/rstb.2010.0045

Sieburth, J. M., Smetacek, V., & Lenz, J. (1978). Pelagic ecosystem structure—Heterotrophic compartments of plankton and their relationship to plankton size fractions. *Limnology & Oceanography*, *23*(6), 1256–1263. https://doi.org/10.4319/lo.1978.23.6.1256

Snyder, W. A., Arnone, R. A., Davis, C. O., Goode, W., Gould, R. W., Ladner, S., et al. (2008). Optical scattering and backscattering byorganic and inorganic particulates in U.S. coastal waters. *Applied Optics*, *47*, 666–677. https://doi.org/10.1364/AO.47.000666

Stramski, D. (1999). Refractive index of planktonic cells as a measure of cellular carbon and chlorophyll a content. *Deep-Sea Research Part I-Oceanographic Research Papers*, *46*(2), 335–351. https://doi.org/10.1016/s0967-0637(98)00065-x

Stramski, D., Boss, E., Bogucki, D., & Voss, K. J. (2004). The role of seawater constituents in light backscattering in the ocean. *Progress in Oceanography*, *61*(1), 27–56. https://doi.org/10.1016/j.pocean.2004.07.001

Stramski, D., & Kiefer, D. A. (1991). Light scattering by microorganisms in the open ocean. *Progress in Oceanography*, *28*, 343–383.

Stramski, D., Reynolds, R. A., Kaczmarek, S., Uitz, J., & Zheng, G. M. (2015). Correction of pathlength amplification in the filter-pad technique for measurements of particulate absorption coefficient in the visible spectral region. *Applied Optics*, *54*(22), 6763–6782. https://doi.org/10.1364/AO.54.006763

Sullivan, J. M., Twardowski, M. S., Ronald, J., Zaneveld, V., & Moore, C. C. (2013). Measuring optical backscattering in water. In A. Kokhanovsky, Ed., *Light scattering reviews 7: Radiative transfer and optical properties of atmosphere and underlying surface* (pp. 189–224). Springer Praxis Books. https://doi.org/10.1007/97836422190786

Sullivan, J. M., Twardowski, M. S., Zaneveld, J. R. V., Moore, C. M., Barnard, A. H., Donaghay, P. L., et al. (2006). Hyperspectral temperature and salt dependencies of absorption by water and heavy water in the 400-750 nm spectral range. *Applied Optics*, *45*(21), 5294–5309. https://doi.org/10.1364/ao.45.005294

Sun, D., Su, X., Wang, S., Qiu, Z., Ling, Z., Mao, Z., & He, Y. (2019). Variability of particulate backscattering ratio and its relations to particle intrinsic features in the Bohai Sea, Yellow Sea, and East China Sea. *Optics Express*, *27*(3), 3074. https://doi.org/10.1364/oe.27.003074

Twardowski, M. S., Boss, E., Macdonald, J. B., Pegau, W. S., Barnard, A. H., & Zaneveld, J. R. V. (2001). A model for estimating bulk refractive index from the optical backscattering ratio and the implications for understanding particle composition in case I and case II waters. *Journal of Geophysical Research-Oceans*, *106*(C7), 14129–14142. https://doi.org/10.1029/2000jc000404

Ulloa, O., Sathyendranath, S., & Platt, T. (1994). Effect of the particle-size distribution on the backscattering ratio in seawater. *Applied Optics*, *33*, 7070–7077.

Werdell, P. J., Proctor, C. W., Boss, E., Leeuw, T., & Ouhssain, M. (2013). Underway sampling of marine inherent optical properties on the Tara Oceans expedition as a novel resource for ocean color satellite data product validation. *Methods in Oceanography*, *7*, 40–51. https://doi.org/10.1016/j.mio.2013.09.001

White, A. E., Letelier, R. M., Whitmire, A. L., Barone, B., Bidigare, R. R., Church, M. J., et al. (2015). Phenology of particle size distributions and primary productivity in the North Pacific subtropical gyre (Station ALOHA). *Journal of Geophysical Research: Oceans*, *120*. https://doi.org/10.1002/2015JC010897

Whitmire, A. L., Boss, E., Cowles, T. J., & Pegau, W. S. (2007). Spectral variability of the particulate backscattering ratio. *Optics Express*, *15*(11), 7019–7031. https://doi.org/10.1364/oe.15.007019

Wozniak, S. B., & Stramski, D. (2004). Modeling the optical properties of mineral particles suspended in seawater and their influence on ocean reflectance and chlorophyll estimation from remote sensing algorithms. *Applied Optics*, *43*(17), 3489–3503. https://doi.org/10.1364/ao.43.003489

Xi, H. Y., Larouche, P., Michel, C., & Tang, S. L. (2015). Beam attenuation, scattering and backscattering of marine particles in relation to particle size distribution and composition in Hudson Bay (Canada). *Journal of Geophysical Research: Oceans*, *120*(5), 3286–3300. https://doi.org/10.1002/2014jc010668

Xi, H., Larouche, P., Tang, S., & Michel, C. (2014). Characterization and variability of particle size distributions in Hudson Bay, Canada. *Journal of Geophysical Research: Oceans*, *119*, 3392–3406. https://doi.org/10.1002/2013JC009542

Zhang, X. D., Hu, L. B., & He, M. X. (2009). Scattering by pure seawater: Effect of salinity. *Optics Express*, *17*(7), 5698–5710. https://doi.org/10.1364/oe.17.005698

Zhang, X. D., Hu, L. B., Xiong, Y. H., Huot, Y., & Gray, D. (2020). Experimental estimates of optical backscattering associated with submicron particles in clear oceanic waters. *Geophysical Research Letters*, *47*(4). https://doi.org/10.1029/2020gl087100